Advanced Powder Technology 33 (2022) 103412

Contents lists available at ScienceDirect

Advanced Powder Technology

journal homepage: www.elsevier.com/locate/apt

Effect of heating conditions on the magnetic properties of micron-sized carboxyl modified-magnetite particles synthesized by a spray pyrolysis and heating process

Masami Hashimoto [a,*], Seiji Takahashi [a], Koichi Kawahara [a], Tomoyuki Ogawa [b], Masakazu Kawashita [c]

[a] Materials Research and Development Laboratory, Japan Fine Ceramics Center, 2-4-1 Mutsuno, Atsuta-ku, Nagoya 456-8587, Japan
[b] Graduate School of Engineering, Tohoku University, 6-6-05 Aoba, Aramaki, Aoba-ku, Sendai 980-8579, Japan
[c] Institute of Biomaterials and Bioengineering, Tokyo Medical and Dental University, 2-3-10 Kanda-Surugadai, Chiyoda-ku, Tokyo 101-0062, Japan

ARTICLE INFO

Article history:
Received 27 August 2021
Received in revised form 13 December 2021
Accepted 22 December 2021
Available online 23 December 2021

Keywords:
Superparamagnetic Fe_3O_4
Spray pyrolysis
Citric acid
Micrometer-sized particle
Heating conditions

ABSTRACT

Superparamagnetic carboxyl (COOH) modified-magnetite (Fe_3O_4) (COOH-Fe_3O_4) micrometer-sized porous particles were synthesized by the spray pyrolysis of a 0.1 M $Fe(NO_3)_3{\cdot}9H_2O$ and 0.2 M citric acid solution and a subsequent heating process in either an Ar + 1% H_2 (P_{O2} = 10^{-20} Pa) or N_2 (P_{O2} = 1 Pa) gas atmosphere. Fe_3O_4 formed due to carbon and hydrogen gas generation of thermal decomposition of citric acid, even under reduction conditions with a P_{O2} below 10^{-23} Pa. The COOH-Fe_3O_4 particles heated in an Ar + 1% H_2 or N_2 atmosphere were porous (40% porosity) and about 1.2 to 1.3 μm in diameter. The particles consist of nano-sized COOH-Fe_3O_4 crystallite about 7 nm in diameter. The specific surface area increased from 116 to 127 m^2/g by increasing the heating time in an Ar + 1% H_2 atmosphere from 10 to 20 h. The saturation magnetization of the COOH-Fe_3O_4 particles (38.7 $A{\cdot}m^2/kg$) heated in Ar + 1% H_2 for 10 h was much higher than that of commercial magnetic microbeads (17 $A{\cdot}m^2/kg$) and the coercivity was 0 kA/m. These superparamagnetic COOH-Fe_3O_4 particles dispersed in distilled water were attracted to a NdFeB magnet for 7–10 s under a 400 Mt external magnetic field, compared with 10 s for commercial magnetic microbeads.

1. Introduction

Magnetic microbeads are becoming increasingly important in diagnostics for detecting viruses [1–7], cancer markers, and hormones using chemiluminescent immunoassays [8–12]. Most applications require superparamagnetic particles with high saturation magnetization because these particles show high dispersibility in solution since they tend to not magnetically interact with each other [13]. Also, highly magnetized particles respond quickly as they generate greater magnetic flux densities when exposed to an applied external magnetic field. Moreover, magnetic microbeads (>1 μm) with a high specific surface area likely adsorb many antibodies towards viruses compared to general magnetic microbeads having a low Fe content and low specific surface area [14–17]. Magnetic microbeads provide separation advantages in solution due to their large diameters (>1 μm), as shown in Equation (1):

$$Fm = (4\pi r^3/3)\, M \text{ grad } H \quad (1)$$

where Fm is the magnetic force, r is the microbead diameter, M is the saturation magnetization, and H is the magnetic field gradient. For example, the particle size of commercial magnetic microbeads, such as MS160/Carboxyl (JSR Life Sciences, Tsukuba, Japan) is 1.6 μm.

Based on this background, preparing spherical and micrometer magnetic particles in a simple, rapid, and harmless process is highly desirable. The spray pyrolysis is an effective method for preparing micrometer-sized particles with spherical shapes in a one-step process at a large scale. The method comprises droplet generation, solvent evaporation, and reaction to product [18–22]. We previously reported the first synthesis of superparamagnetic carboxyl (COOH) modified-magnetite (Fe_3O_4) (COOH-Fe_3O_4) micrometer-sized porous particles by spray pyrolysis and a subsequent heating process (unpublished results). The starting reagents were 0.1 M $Fe(NO_3)_3{\cdot}9H_2O$ solution and 0.15 M citric acid (CA) (CA/Fe = 1.5). The saturation magnetization (Ms) of the synthesized beads (51 $A{\cdot}m^2/kg$) is much higher than that of commercial magnetic microbeads (17 $A{\cdot}m^2/kg$), and their coercivity is 0.24 kA/m.

* Corresponding author.
E-mail address: masami@jfcc.or.jp (M. Hashimoto).

https://doi.org/10.1016/j.apt.2021.103412

The specific surface area is 109.3 m^2/g, which is thirty times higher than that of commercial microbeads. In contrast, ferromagnetic COOH-Fe_3O_4 micrometer-sized dense particles were formed (CA/Fe = 1). Ms of these beads is 19 $A{\cdot}m^2/kg$ and their coercivity is 5.5 kA/m. The specific surface area is 14.0 m^2/g [1–34]. In the spray pyrolysis process, a solution of $Fe(NO_3)_3{\cdot}9H_2O$ and CA misted into droplets is carried by gas into a hot zone, where they are rapidly heated and decompose to form an amorphous product and CA residue composites [23,24]. Subsequent heating in Ar + 1% H_2 atmosphere for 10 h results in the crystallization of Fe_3O_4 and decomposition of CA. A high CA content (CA/Fe = 1.5) clearly enhances the evaporation and decomposition of CA, resulting in the formation of a large number of pores on the surface and inside of the aerosol particles. Thus, it is considered that the larger CA/Fe effect on the magnetic and particle properties such as specific surface area of COOH-Fe_3O_4 particles.

The spray pyrolysis process typically forms sub-micrometer- to micrometer-sized particles, which is adequate for magnetic bioseparation. The micron-sized particles consist of multiple nano-sized crystallites which form a three-dimensional network [23,24]. We, therefore, attempted to prepare micron-sized magnetic particles consisting of multiple nano-sized crystallites exhibiting superparamagnetic properties. In general, superparamagnetic properties of Fe_3O_4 require small crystallites ranging from 1 to 30 nm [13]. We recently showed by transmission electron micrographic observation that the crystallite size of superparamagnetic COOH-Fe_3O_4 particles (CA/Fe = 1.5) is about 9 nm, and the edge-to-edge separation of the crystallites is about 8 nm (unpublished results). In contrast, the crystallite size of ferromagnetic COOH-Fe_3O_4 particles (CA/Fe = 1) is about 3 nm, and the edge-to-edge separation of the crystallites is about 3.2 nm. Superparamagnetic particles likely exhibit both increased dispersibility of COOH-Fe_3O_4 crystallites below 30 nm in diameter and tend to not magnetically interact with each other.

Superparamagnetic COOH-Fe_3O_4 particles hold promise as magnetic beads for chemiluminescent immunoassays. However, the mobility of COOH-Fe_3O_4 particles in solution and the ability of antibodies to bind to the particles also depends on the specific surface area, COOH group content, and magnetic properties. In particular, Fe_3O_4 formation depends on the partial oxygen pressure (P_{O2}) of the atmosphere and temperature [25]. The spray pyrolysis using reducing agents such as ethanol, ethylene glycol, and formic acid is useful for hydrogen gas generation of thermal decomposition of reduction agents [26]. Thus, CA is also considered to be useful for reduction agents for the generation of hydrogen gas. However, higher content of CA, the heating condition such as partial oxygen pressure (P_{O2}) of atmosphere on the magnetic and particle properties such as specific surface area has not been reported.

In the present study, we prepared micrometer-sized porous particles by spray pyrolysis using a higher CA content and a subsequent heating process. We investigated the effect of heating conditions, such as various P_{O2} values and heating time in the kiln furnace, on the microstructure and magnetic properties of the resulting COOH-Fe_3O_4 particles.

2. Materials and methods

2.1. Synthesis of Fe_3O_4 porous particles

$Fe(NO_3)_3{\cdot}9H_2O$ (99.9%) was purchased from Fujiwako-Chemicals (Osaka, Japan).

Citric acid (99.9%) was purchased from Kanto Chemicals (Tokyo, Japan). $Fe(NO_3)_3{\cdot}9H_2O$ (0.1 M) and citric acid (0.2 M) were dissolved in water. This metal precursor solution was then atomized using an ultrasonic wave generator and the mist was reacted in a four-zone furnace at 423, 473, 573, and 673 K under airflow (10 L/min). The produced precursor powders synthesized by spray pyrolysis were heated to crystallize the precursor powders and decompose CA in the kiln furnace at 573 K for 10 or 20 h in an Ar + 1% H_2 or N_2 gas atmosphere and their flow rates were 0.05 L/min. The sample names and heating conditions in the kiln furnace for each sample are shown in Table 1. The P_{O2} of the Ar + 1% H_2 and N_2 gas measured by ZrO_2-type oxygen sensor (Daiichinekken Co., Ltd., Hyogo, Japan) at 1011 K were 10^{-20} and 1 Pa, respectively, and their flow rates were 0.05 L/min.

2.2. Analysis of the synthesized particles

The precursor and heat-treated powders were analyzed by powder X-ray diffraction (XRD) using a RINT Model 2000 spectrometer (Rigaku Denki Co., Ltd., Tokyo, Japan) with a CuKα X-ray source operated at 40 kV and 40 mA. The crystallite size was estimated by Scherrer's equation. Fourier transforms infrared (FT-IR) spectra of the precursor and heat-treated powders were analyzed by the KBr method using an FT-IR/NIR Spectrometer Frontier (Perkin Elmer Co., Ltd., Kanagawa, Japan) to confirm the functional groups in the powders. The C and Fe content (wt %) of the particles was examined using a combustion infrared absorption method using an EMIA-110 (HORIBA Ltd., Kyoto, Japan) according to JIS R 1603 [27] and inductively coupled plasma emission spectrometry using an IRIS Advantage ICAP (Thermo Fisher Scientific Inc. Waltham, MA, USA), respectively. The C/Fe atomic ratio was calculated.

Scanning electron microscopy (SEM) images of the surfaces and cross-sections of the heat-treated particles were obtained to examine the morphology of the particles. For cross-sectional observation, the particles were embedded in a resin and sectioned by argon milling with an IM4000 (Hitachi Co., Ltd., Tokyo, Japan). The porosity of the heat-treated particles was obtained by cross-sectional SEM image analysis (n = 3). The cross-sectional SEM image of the particles was converted into a binarized image. The number of black pixels, which corresponded to the pores, in the converted image was counted. Then, the porosity was measured as the ratio of black pixels against total pixels.

The size distribution of the heat-treated particles was determined by image analysis of 20,000 particles, using a Morphologi 4-ID (Malvern Panalytical Ltd., Tokyo, Japan). For comparison, the particle size distribution of a commercial magnetic particle product, MS160/Carboxyl was also determined. The specific surface area of the heat-treated particles was determined using Brunauer-Emmett-Teller (BET) theory and a sorption analyzer (BELSORP-mini II, MicrotracBEL, Osaka, Japan). The tap density of the COOH-Fe_3O_4 particles was determined according to JIS R 1628 [28].

2.3. Magnetic properties of the particles

The Ms and coercive force (Hc) of the heat-treated particles were characterized from the hysteresis loop measured using a vibrating sample magnetometer (VSM) (PPMS-VersalabTM, Quantum Design, Tokyo, Japan) in magnetic fields up to 10 kA/m at

Table 1
Heating conditions used to generate the particles synthesized by spray pyrolysis in a kiln furnace.

Sample	Heating condition in kiln furnace		
	Gas	Temp (K)	Holding time (h)
Precursor	–	–	–
N-10h	N_2	573	10
H-10h	Ar + 1% H_2	573	10
H-20h	Ar + 1% H_2	573	20

room temperature. Ms is the value at 2000 kA/m. For comparison, commercial MS160/Carboxyl was also characterized.

3. Results and discussion

Fig. 1 shows the XRD patterns of the precursor and heat-treated particles. The precursor powder synthesized by spray pyrolysis was an amorphous-type product (Fig. 1(a)). In contrast, Fe_3O_4 single phases (ICDD card #19-0629) with higher crystallinity were formed after heating in either an N_2 (P_{O2}: 1 Pa) or Ar + 1% H_2 atmosphere (P_{O2}: 10^{-20} Pa) at 573 K for 10 or 20 h (crystallite sizes of 7.22 (b), 7.09 (c) and 7.56 (d) nm, as estimated by Scherrer's formula). Fe_3O_4 is generally formed in a reducing atmosphere with a P_{O2} of 10^{-35} to 10^{-23} Pa at 573 K [25]. Interestingly, a Fe_3O_4 single phase was formed in both Ar + 1% H_2 (P_{O2}: 10^{-20} Pa) and N_2 (P_{O2}: 1 Pa) atmosphere, irrespective of the P_{O2} value above 10^{-23} Pa. Therefore, pyrolysis and heating residues such as carbon [29] formed in the particles and hydrogen gas generation [26] of thermal decomposition of CA are likely useful for attaining a reducing atmosphere under a P_{O2} of 10^{-35} to 10^{-23} Pa to form Fe_3O_4.

Fig. 2 shows the FT-IR spectra of the precursor and heat-treated particles. A strong adsorption band around 570 cm^{-1} relates to the vibration of the Fe—O functional group [30] of Fe_3O_4 and is observed for all particles, clearly indicating the presence of the Fe_3O_4 or Fe_3O_4 precursor. Three adsorption bands around 1410, 1545, and 2940 cm^{-1} related to the carboxylate group of CA [31] are observed for all particles, indicating residual CA after thermal pyrolysis. The intensities of these peaks are largest in the precursor particles and decrease the following heating in the kiln furnace. Heating of the Fe_3O_4 precursors provided new bands at 1610 and 1720 cm^{-1} [32–34] (Fig. 2 (b)-(d)) absent in the precursor spectrum (Fig. 2 (a)), confirming an interaction between the Fe atoms of Fe_3O_4 and the carboxylate group of CA that provides fractional single bond character to the carbonyl. This FT-IR spectra data showed introducing the COOH group to the surface and inside of Fe_3O_4 particles. However, it is essential to evaluate the amount of COOH group and antigen–antibody reaction for chemiluminescent immunoassays in the near future.

During the spray pyrolysis process, when the particle temperature exceeds the melting point of CA at 426 K, the CA melts and

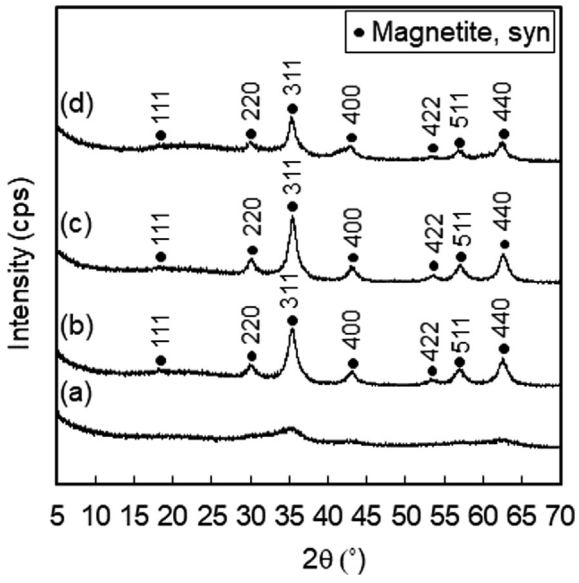

Fig. 1. Powder XRD patterns of particles synthesized by the spray pyrolysis and heating process. a) Precursor, b) N-10h (7.22 nm), c) H-10h (7.09 nm), and d) H-20h (7.56 nm). The crystalline sizes obtained by XRD are given in parentheses.

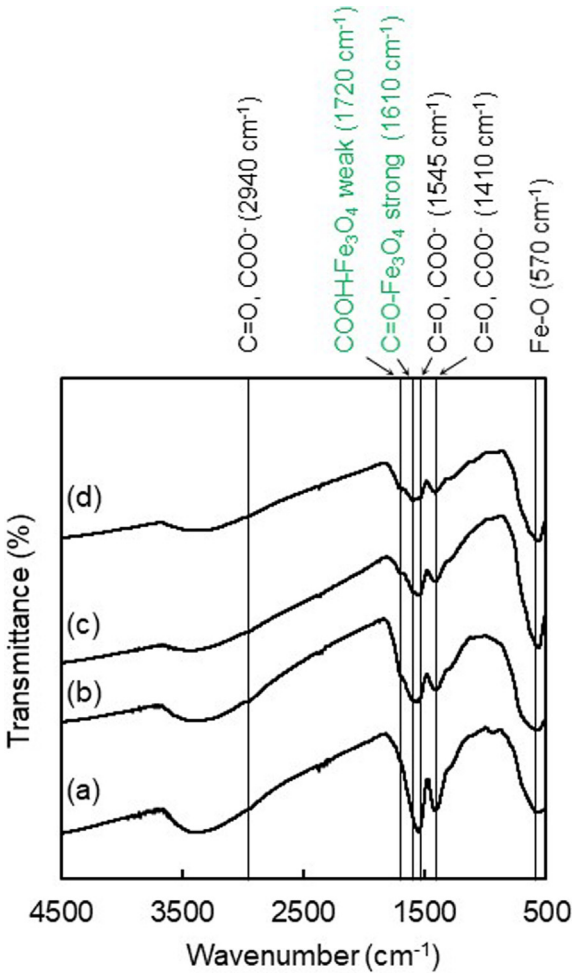

Fig. 2. FT-IR spectra of particles synthesized by the spray pyrolysis and heating process. a) Precursor, b) N-10h, c) H-10h, and d) H-20h.

acts as a high-temperature solvent. The reactants can then dissolve, react, and, upon exceeding the solubility limit, precipitate in the solvent [24]. These processes can remarkably enhance mass transfer due to the liquid-state solvent. Since CA can spontaneously diffuse onto many Fe_3O_4 crystallites, CA can wet the surface of the crystallites, possibly aiding the dispersion of the crystallites in the secondary particles. Moreover, aerosol particles suspended in the air at 423 to 673 K undergo the CA and Fe_3O_4 precursor reaction, dispersion, and CA evaporation and decomposition. If a large amount of CA pyrolysis residue remains in the secondary COOH-Fe_3O_4 particles, the content of C which was derived from CA against Fe is high. The C and Fe content of the particles was examined using infrared absorption and inductively coupled plasma emission spectrometry, respectively. The C/Fe atomic ratios of COOH-Fe_3O_4 particles for precursor, N-10h, H-10h, and H-20h were 1.30 ± 0.03, 0.87 ± 0.01, 0.89 ± 0.02, and 0.80 ± 0.01 (n = 3), respectively, revealing that more CA remained in the precursor secondary particles than in heat-treated particles. The evaporation and decomposition of CA were enhanced with increased heating time.

Fig. 3 shows surface and cross-sectional SEM images of N-10h (a), H-10h (b), and H-20h (c) particles. Spherical and porous COOH-Fe_3O_4 particles were formed in all cases. The microstructure of the COOH-Fe_3O_4 particles was similar, irrespective of the heating atmosphere and temperature and thus the microstructure of COOH-Fe_3O_4 particles depends on the CA/Fe ratio (unpublished results). The secondary particle size distribution was almost the same for N-10h (1.28 ± 0.34 μm), H-10h (1.26 ± 0.32 μm), and

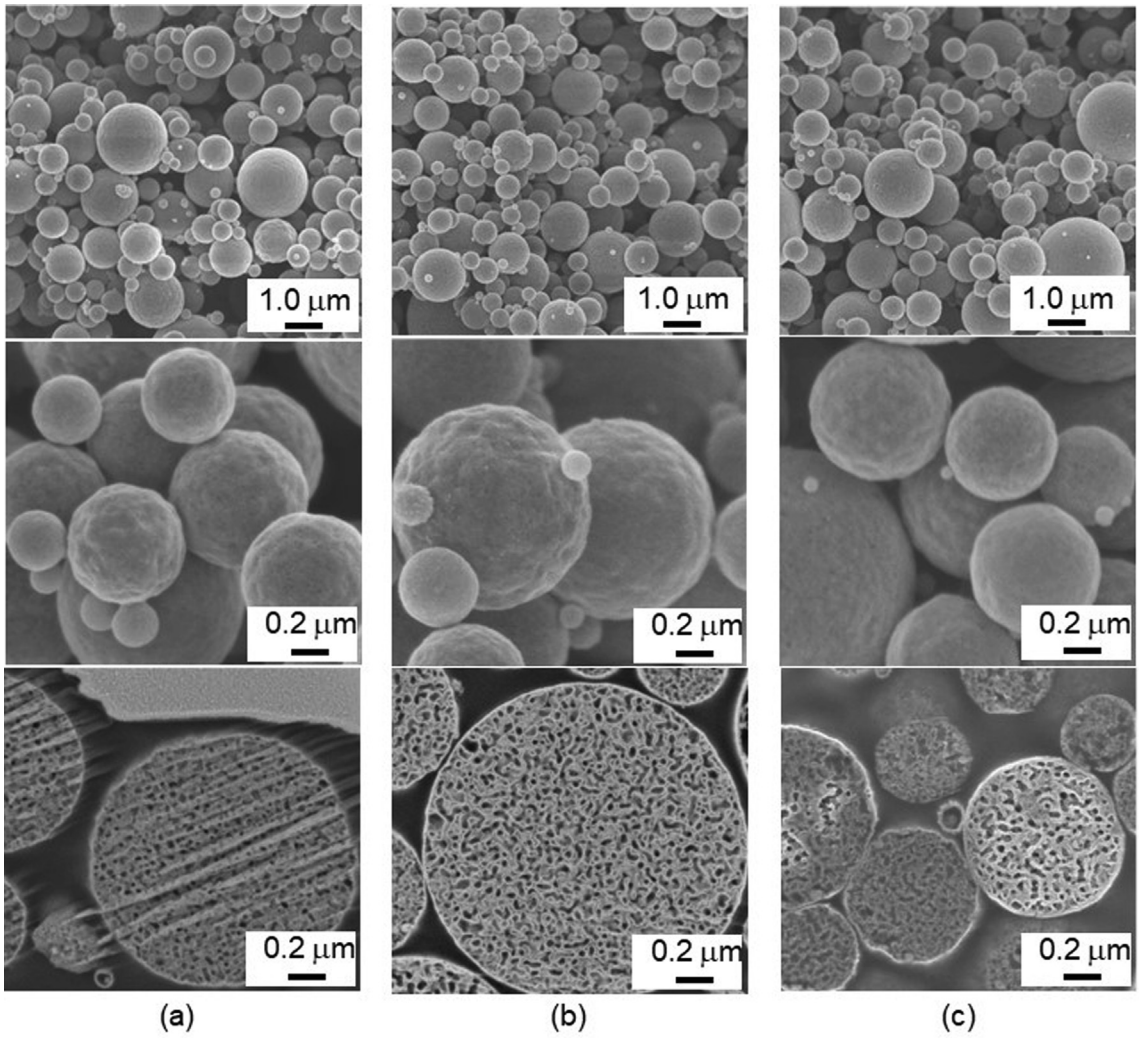

Fig. 3. SEM images of the surface (upper and middle) and cross-sections (bottom) of COOH-Fe_3O_4 particles synthesized by the spray pyrolysis and heating process. (a) N-10h, (b) H-10h, and (c) H-20h.

H-20h (1.31 ± 0.42 μm), whereas MS160/Carboxyl (1.68 ± 0.38 μm) was larger than that of COOH-Fe_3O_4 particles (Fig. 4). The BET surface areas were 103.0, 116.2, and 126.9 m^2/g for N-10h, H-10h and H-20h, respectively. The specific surface areas of these COOH-Fe_3O_4 particles increased with increasing time and were thirty

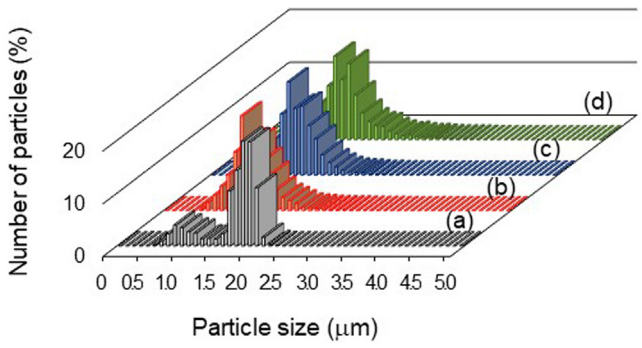

Fig. 4. Secondary particle size distribution of COOH-Fe_3O_4 particles synthesized by the spray pyrolysis and heating process. (a) Commercial MS160/Carboxyl (1.68 ± 0.38 μm), (b) N-10h (1.28 ± 0.34 μm), (c) H-10h (1.26 ± 0.32 μm), and (d) H-20h (1.31 ± 0.42 μm). The average particle size and standard deviation are given in parenthesis.

times larger than that of the commercial product MS160/Carboxyl (3.4 m^2/g). Clearly, a CA content (CA/Fe = 2) enhances the evaporation and decomposition of CA, resulting in the formation of many pores inside of the COOH-Fe_3O_4 particles. The porosity of the COOH-Fe_3O_4 particles estimated from the cross-sectional SEM images in Fig. 3(b) for H-10h was 40 %, which is larger than that of previously reported COOH-Fe_3O_4 (CA/Fe = 1.5, porosity 39 %, specific surface area 109.2 m^2/g) (unpublished results). The heating condition of CA/Fe = 1.5 was the same as that of H-10h. The higher porosity of CA/Fe is useful for forming COOH-Fe_3O_4 particles with a high specific surface area. Thus, the tap density of H-10h (0.48 g/cm^3) was smaller than that of COOH-Fe_3O_4 (CA/Fe = 1.5, 0.69 g/cm^3).

The magnetic properties of COOH-Fe_3O_4 and commercial MS160/Carboxyl particles were determined by VSM analysis at room temperature. The saturation magnetization as a function of the applied magnetic field is shown in Fig. 5. The magnetization curve shows superparamagnetic behavior for all COOH-Fe_3O_4 particles. The saturation magnetization was 35.7, 38.7 and 35.2 $A{\cdot}m^2/kg$ for N-10h, H-10h, and H-20h, respectively, which are larger than that of the commercial product MS160/Carboxyl (16.7 $A{\cdot}m^2/kg$) but smaller than that of COOH-Fe_3O_4 particles (CA/Fe = 1.5) (unpublished results). This is due to the high C/Fe value of COOH-Fe_3O_4 (CA/Fe = 2) compared with that of COOH-Fe_3O_4 particles

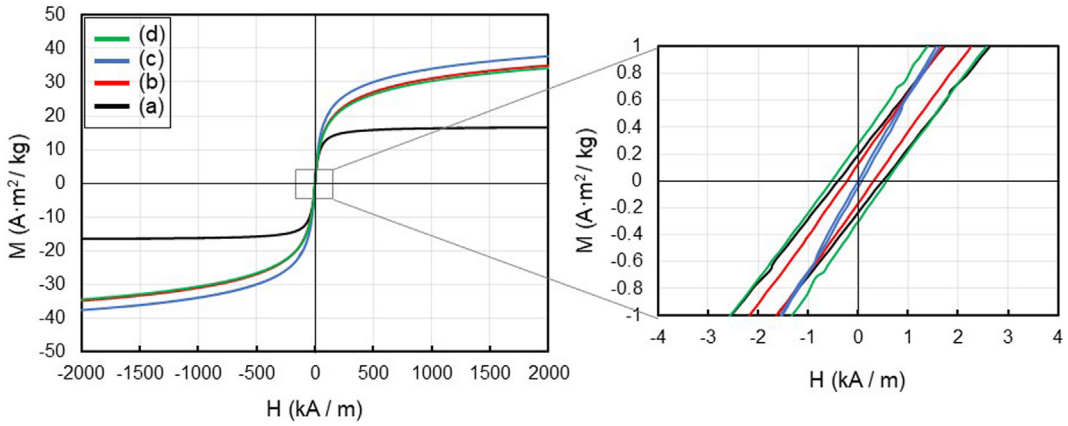

Fig. 5. VSM spectra of COOH-Fe_3O_4 particles synthesized by the spray pyrolysis and heating process. (a) Commercial MS160/Carboxyl, (b) N-10h, (c) H-10h, and (d) H-20h.

(CA/Fe = 1.5). No hysteresis or remanence was observed, and the behavior was completely reversible at 300 K. The coercivity for N-10h, H-10h, and H-20h was 0.3, 0, and 0.56 kA/m, respectively, N-10h and H-10h are smaller than that of the commercial product MS160/Carboxyl (0.48 kA/m). We previously reported that the superparamagnetic properties of COOH-Fe_3O_4 particles are due to the COOH-Fe_3O_4 crystallites being below 10 nm in diameter, and these crystallites are dispersed in the secondary particles and do not magnetically interact with each other. In this study, the crystallites for N-10h, H-10h and H-20h were about 7 nm in diameter, as estimated from Fig. 1. Although the edge-to-edge separation was not measured, crystallites about 7 nm in diameter dispersed in the secondary particles and did not interact magnetically.

Fig. 6 shows a digital photo image of a suspension of H-10h in distilled water (a), the magnetic attraction of H-10h particles (2 mg/2 ml) (b), and H-10h resuspension after pipetting (c). The superparamagnetic COOH-Fe_3O_4 particles of H-10h could be dispersed in distilled water after sonication for 10 min, and the resultant suspension responded to an external magnetic field of 400 mT (Nd-Fe-B magnet) for 7–10 s (compared to 10 s for commercial MS-160/Carboxyl). H-10h particles were redispersed in distilled water after pipetting due to their superparamagnetic property.

4. Conclusion

Superparamagnetic micron-sized COOH-Fe_3O_4 porous particles were synthesized by spray pyrolysis of 0.1 M $Fe(NO_3)_3{\cdot}9H_2O$ and 0.2 M citric acid solution, followed by heating either under an Ar + 1% H_2 (P_{O2}: 10^{-20} Pa) or N_2 (P_{O2}: 1 Pa) gas atmosphere at 573 K for 10 or 20 h. In general, Fe_3O_4 is formed in a reducing atmosphere with a P_{O2} of 10^{-35} to 10^{-23} Pa at 573 K. In this work, the reduction condition for forming Fe_3O_4 was probably attained by carbon residue derived from the thermal pyrolysis of CA and hydrogen gas generation of thermal decomposition of CA. The microstructure of the COOH-Fe_3O_4 particles was porous (40% porosity) and the specific surface area was about 120 m^2/g. This high specific surface area was due to the inside pores of COOH-Fe_3O_4 particles. The saturation magnetization of the COOH-Fe_3O_4 particles was almost 39 $A{\cdot}m^2/kg$, which is much higher than that of commercial magnetic microbeads (17 $A{\cdot}m^2/kg$). The superparamagnetic H-10h COOH-Fe_3O_4 particles dispersed in distilled water; were attracted to a magnet and redispersed upon pipetting after removing the magnet. The content of the COOH group and the antigen–antibody reaction of superparamagnetic porous COOH-Fe_3O_4 particles should be examined in the near future.

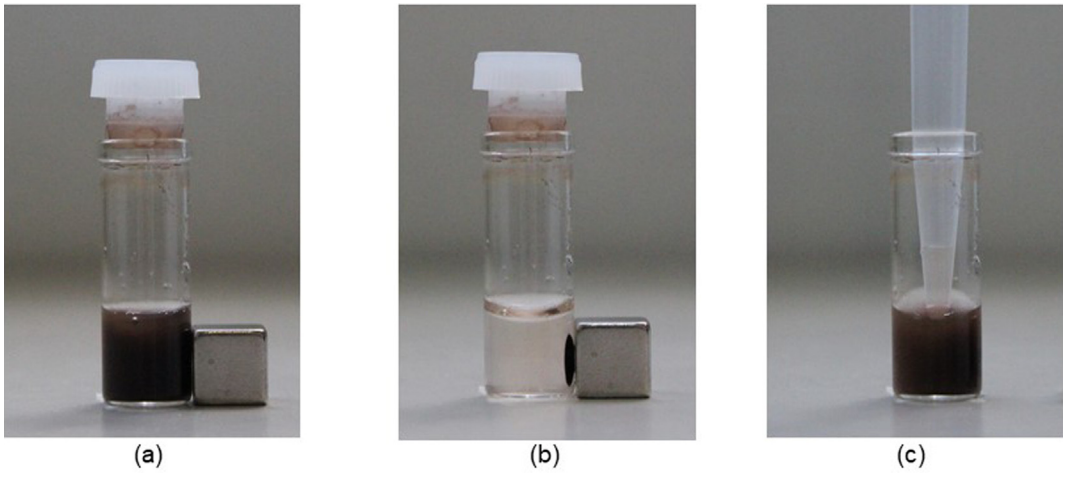

Fig. 6. Digital photographs of (a) H-10h suspension in distilled water, (b) magnetic attraction of H-10h particles, and (c) H-10h resuspension after pipetting.

Declaration of Competing Interest

The authors declare that they have no known competing financial interests or personal relationships that could have appeared to influence the work reported in this paper.

Acknowledgments

The authors thank Y. Miyanagi for helpful discussions and experimental support (The Kansai Electric Power Co., Inc., Hyogo, Japan).

References

[1] K. Satoh, A. Iwata, M. Murata, M. Hikata, T. Hayakawa, T. Yamaguchi, Virus concentration using polyethyleneimine-conjugated magnetic beads for improving the sensitivity of nucleic acid amplification tests, J. Virol. Methods. 114 (2003) 11–19.
[2] A. Iwata, K. Satoh, M. Murata, M. Hikata, T. Hayakawa, T. Yamaguchi, Virus concentration using sulfonated magnetic beads to improve sensitivity in nucleic acid amplification tests, Biol. Pharm. Bull. 26 (8) (2003) 1065–1069.
[3] E. Uchida, M. Kogi, T. Oshizawa, B. Furuta, K. Satoh, A. Iwata, M. Murata, M. Hikata, T. Yamaguchi, Optimization of the virus concentration method using polyethyleneimine-conjugated magnetic beads and its application to the detection of human hepatitis A, B and C viruses, J. Virol. Methods. 143 (1) (2007) 95–103.
[4] A. Sakudo, K. Ikuta, Efficient capture of infectious H5 avian influenza virus utilizing magnetic beads coated with anionic polymer, Biochem. Biophys. Res. Commun. 377 (1) (2008) 85–88.
[5] W.-S. Chang, H. Shang, R.M. Perera, S.-M. Lok, D. Sedlak, R.J. Kuhn, G.U. Lee, Rapid detection of dengue virus in serum using magnetic separation and fluorescence detection, Analyst. 133 (2) (2008) 233–240.
[6] G.D. Chen, C.J. Alberts, W. Rodriguez, M. Toner, Concentration and purification of human immunodeficiency virus Type 1 virions by microfluidic separation of superparamagnetic nanoparticles, Anal. Chem. 82 (2) (2010) 723–728.
[7] A. Sakudo, K. Baba, M. Tsukamoto, A. Sugimoto, T. Okada, T. Kobayashi, N. Kawashita, T. Takagi, K. Ikuta, Anionic polymer, poly (methyl vinyl ether–maleic anhydride)-coated beads-based capture of human influenza A and B virus, Bioorg. Med. Chem. 17 (2) (2009) 752–757.
[8] M. Kalos, B.L. Levine, D.L. Porter, S. Katzs, S.A. Grupp, A. Bagg, C.H. June, T cells with chimeric antigen receptors have potent antitumor effects and can establish memory in patients with advanced leukemia, Sci. Transl. Med. 3 (2011) 95ra73.
[9] B.P. Casavant, R. Mosher, J.W. Warrick, L.J. Maccoux, S.M.F. Berry, J.T. Becker, V. Chen, J.M. Lang, D.G. McNeel, D.J. Beebe, A negative selection methodology using a microfluidic platform for the isolation and enumeration of circulating tumor cells, Methods 64 (2013) 137–143.
[10] A. Chen, T. Byvank, W.-J. Chang, A. Bharde, G. Vieira, B.L. Miller, J.J. Chalmers, R. Bashir, R. Sooryakumar, On-chip magnetic separation and encapsulation of cells in droplets, Lab Chip. 13 (6) (2013) 1172, https://doi.org/10.1039/c2lc41201b.
[11] N.M. Adams, H. Bordelon, K.-K. Wang, L.E. Albert, D.W. Wright, F.R. Haselton, Comparison of three magnetic bead surface functionalities for RNA extraction and detection, ACS Appl. Mater. 7 (11) (2015) 6062–6069.
[12] L. Borlido, A.M. Azevedo, A.C.A. Roque, M.R. Aires-Barros, Magnetic separations in biotechnology, Biotechnol. Adv. 31 (8) (2013) 1374–1385.
[13] D. Horák, M. Babič, H. Macková, M.J. Beneš, Preparation and properties of magnetic nano- and microsized particles for biological and environmental separations, J. Sep. Sci. 30 (11) (2007) 1751–1772.
[14] J. Chatterjee, Y. Haik, C.-J. Chen, Synthesis and characterization of heat-stabilized albumin magnetic microspheres, Colloid. Polym. Sci. 279 (11) (2001) 1073–1081.
[15] D. Tanyolac, A.R. Ozdural, New low cost magnetic material: Magnetic polyvinylbutyral microbeads, React. Funct. Polym. 43 (2000) 279–286.
[16] F. Sauzedde, A. Elaïssari, C. Pichot, Hydrophilic magnetic polymer latexes. 2. encapsulation of adsorbed iron oxide nanoparticles, Colloid. Polym. Sci. 277 (11) (1999) 1041–1050.
[17] F. Sauzedde, A. Elaïssari, C. Pichot, Hydrophilic Magnetic Polymer Latexes. 1. Adsorption of magnetic iron oxide nanoparticles onto various cationic latexes, Colloid. Polym. Sci. 277 (9) (1999) 846–855.
[18] A. Gurav, T. Kodas, T. Pluym, Y. Xiong, Aerosol processing of materials, Aerosol Sci. Technol. 19 (4) (1993) 411–452.
[19] K. Okuyama, I. Wuled Lenggoro, Preparation of nanoparticles via spray route, Chem. Eng. J. 58 (3-6) (2003) 537–547.
[20] D.S. Jung, S.B. Park, Y.C. Kang, Design of particles by spray pyrolysis and recent progress in its application, Korean J. Chem. Eng. 27 (6) (2010) 1621–1645.
[21] T. Ogi, A.B.D. Nandiyanto, K. Okuyama, Nanostructuring strategies in functional fine-particle synthesis towards resource and energy saving applications, Adv. Powder Technol. 25 (1) (2014) 3–17.
[22] T. Ogi, H. Fukazawa, A.M. Rahmatika, T. Hirano, K.L.A. Cao, F. Iskandar, Improving the crystallinity and purity of monodisperse Ag fine particles by heating colloidal sprays in-flight, Ind. Eng. Chem. Res. 59 (2020) 5745–5751.
[23] G.L. Messing, S.C. Zhang, G.V. Jayanthi, Ceramic powder synthesis by spray pyrolysis, J. Am. Ceram. Soc. 76 (1993) 2707.
[24] I.W. Lenggoro, T. Hata, F. Iskandar, M.M. Lunden, K. Okuyama, An experimental and modeling investigation of particle production by spray pyrolysis using a laminar flow aerosol reactor, J. Mater. Res. 15 (3) (2000) 733–743.
[25] A. Muan, Phase equilibria at high temperatures in iron silicate systems, Am. Ceram. Soc. Bull. 37 (1958) 81–84.
[26] E.L. Septiani, J. Kikkawa, K.L.A. Cao, T. Hirano, N. Okuda, H. Matsumoto, Y. Enokido, T. Ogi, Direct synthesis of submicron FeNi particles via spray pyrolysis using various reduction agents, Adv. Powder Technol. 32 (11) (2021) 4263–4272.
[27] Japanese Industrial Standards (JIS), Methods for chemical analysis of fine silicon nitride powders for fine ceramics (JIS R 1603:2007).
[28] Japanese Industrial Standards (JIS), Test methods for bulk density of fine ceramic powder (JIS R 1628:1997).
[29] M.M. Rahman, S.-L. Chou, C. Zhong, J.-Z. Wang, D. Wexler, H.-K. Liu, Spray pyrolyzed NiO–C nanocomposite as an anode material for the lithium-ion battery with enhanced capacity retention, Solid State Ionics 180 (40) (2010) 1646–1651.
[30] M. Yamaura, R.L. Camilo, L.C. Sampaio, M.A. Macêdo, M. Nakamura, H.E. Toma, Preparation and characterization of (3-aminopropyl) triethoxysilane-coated magnetite nanoparticles, J. Magn. Magn. Mater. 279 (2-3) (2004) 210–217.
[31] L.C. Bichara, H.E. Lanús, E.G. Ferrer, M.B. Gramajo, S.A. Brandán, Vibrational Study and Force Field of the Citric Acid Dimer Based on the SQM Methodology, Adv. Phys. Chem. 2011 (2011) 1–10.
[32] R.M. Silverstein, G.C. Bassler, T.C. Morrill, Spectrometric identification of organic compounds, 4th ed., John Wiley & Sons, 1981.
[33] M. Arefi, M. Kazemi Miraki, R. Mostafalu, M. Satari, A. Heydari, Citric acid stabilized on the surface of magnetic nanoparticles as an efficient and recyclable catalyst for transamidation of carboxamides phthalimide, urea and thiourea with amines under neat conditions, J. Iran. Chem. Soc. 16 (2) (2019) 393–400.
[34] D. Singh, R.K. Gautam, R. Kumar, B.K. Shukla, V. Shankar, V. Krishna, Citric acid coated magnetic nanoparticles: Synthesis, characterization and application in removal of Cd(II) ions from aqueous solution, J. Water Process Eng. 4 (2014) 233–241.